Tides Need STEMMED: A Locally Operating Spatio-Temporal Mutually Exciting Point Process with Dynamic Network for Improving Opioid Overdose Death Prediction

Che-Yi Liao[1], Gian-Gabriel Garcia, Kamran Paynabar, Zheng Dong, Yao Xie
H. Milton Stewart School of Industrial and Systems Engineering
Georgia Institute of Technology
Atlanta
[1]{cyliao}@gatech.edu

Mohammad S. Jalali
Massachusetts General Hospital
Harvard Medical School
Boston, MA, USA

ABSTRACT

Problem definition: Efforts to mitigate the U.S. opioid crisis have been complicated by ever-changing trends in opioid overdose deaths (OODs) across communities and drug types. Public health surveillance efforts are challenged with variability among these factors, making prediction of local OOD trends and coordination across communities critical. In this research, we design a model capable of leveraging implicit connections between past- and future-OODs, operating across locales, and providing accurate local and global forecasts of OOD trends. **Methodology/results:** We develop a Spatio-TEMporal Mutually Exciting point process with Dynamic network (STEMMED), i.e., a point process network wherein each node models a unique community-drug event stream with a dynamic mutually-exciting structure, accounting for influences from other nodes. We show that STEMMED can be decomposed node-by-node, suggesting a tractable distributed learning procedure. Simulation shows that this learning algorithm can accurately recover known parameters of STEMMED, especially for small networks and long data-horizons. Next, we turn this node-by-node decomposition into an online cooperative multi-period forecasting framework, which is asymptotically robust to operational errors, to facilitate OOD trends forecasting among neighboring communities. In our numerical study, we parameterize STEMMED using individual-level OOD data and county-level demographics in Massachusetts. For any node, we observe that OODs within the same drug class from nearby locations have the greatest influence on future OOD trends. Furthermore, the expected proportion of OODs triggered by historical events varies greatly across counties, ranging between $30\% - 70\%$. Finally, in a practical online forecasting setting, STEMMED-based cooperative framework reduces prediction error by 60% on average, compared to well-established forecasting models. **Managerial implications:** Leveraging the growing abundance of public health surveillance data, STEMMED can provide accurate forecasts of local OOD trends and highlight complex interactions between OODs across communities and drug types. Moreover, STEMMED enhances synergies between local and federal government entities, which is critical to designing impactful policy interventions.

1 Introduction

The current opioid crisis has been identified as one of the most severe public health crises in United States (US) history [Volkow and Blanco, 2021]. Despite the increasing amount of public and private resources dedicated to preventing opioid overdose deaths (OODs), the situation has become worse [Gussow, 2016]. In 2019, 70% of the $70,000$ drug overdose deaths were associated with opioids, and in 2020 around $65,000$ deaths were identified to be opioid-related, representing 77% of the total drug overdose deaths [National Center for Health Statistics (NCHS), 2021].

Accurate forecasts of overall OOD trends are critical to facilitate effective public health policy planning on both local and national scales [Bharat et al., 2021]; however, surveillance efforts have been complicated by the ever-changing drug overdose trends across various geographic regions and population groups [Dembek et al., 2020, Volkow and Blanco, 2021]. Retrospective analyses have shown that the U.S. has suffered three waves of the opioid crisis, each of which had distinctive major causes. The first wave, which started around 2000, was mainly due to increased prescription of opioids. However, due to their increased accessibility, the second and third waves (which started a decade later) were predominantly driven by illicitly manufactured Heroin and Fentanyl [Volkow and Blanco, 2021]. More recently, increasing fatalities of psychostimulants-involved OODs has signaled a new wave of the OOD crisis [Ciccarone, 2021]. Due to their vastly differing origins, it has been extremely challenging to estimate future OOD progressions. Additionally, detecting new trends from data is challenging because the average lag time (i.e., the time between when the death occurred and when the data are available for analysis) is 4 to 6 months. This data recording delay often follows with a reporting delay, ranging from a few months to two years across various states. [Bharat et al., 2021, Ahmad et al., 2022]. These challenges have stifled policy efforts by the local, state, and federal governments to mitigate the lurking threats of OODs [Vadivelu et al., 2018]. As such, accurate long-term forecasts of overall OOD trends have become necessary for public health policymaking.

Moreover, projecting OOD trends at the local level (e.g., county) could be formidable given the geographically and socioeconomically diverse OOD trends [Scholl et al., 2019, Mattson et al., 2021]. For example, evidence shows that poor and affluent areas are generally concerned with OODs with different drugs [Pear et al., 2019]. These differences are further complicated by racial disparities in opioid-related morbidity and mortality [Lippold et al., 2019, Altekruse et al., 2020, Liao et al., 2022]. Critically, OODs tend to happen in proximity to each other [Carter et al., 2019, Hernandez et al., 2020]. The heterogeneous characteristics of OODs necessitate a tailored response by local public health departments and the federal government. We posit that the development of cross-system forecasting approaches that facilitates cooperation across local communities is critical to address the opioid crisis at local and state levels [Johnson et al., 2018]. However, how to design such a forecasting system remains an open question.

To address the burning need of a systemically designed forecasting model that can be maintained locally, we propose a novel Spatio-TEMporal Mutually Exciting point process with Dynamic network (STEMMED). STEMMED models the dynamic connections between individual OODs through an elegant functional structure that reflects the observations of the space-time clustered OODs. Moreover, STEMMED is coupled with community-level spatial covariates and individual-level socioeconomic information, thereby empowering strong performance in both short- and long-term forecasting. STEMMED can be *localized*, i.e., be decomposed into and operated at various community levels, which enables efficient and effective collective policy design for local public health departments.

1.1 Related Works

Predictive Models for the Opioid Crisis. Researchers have attempted to reproduce the complex OOD progressions via carefully calibrated simulation models. Pitt et al. [2018] used a compartmental model to simulate addiction-related OODs in various pain, opioid use, and health states. Homer and Wakeland [2021] considered changing system dynamics that captures snowball effect of social influence. With a more operationally detailed and data-driven compartmental model, Lim et al. [2022] and Stringfellow et al. [2022] described a system involving opioid misuse initiation, opioid use disorder, treatment, and remission. However, none of these works considered the great heterogeneity existing at state or local levels in regard to the burden and dynamics of the opioid crisis. This shortage is in fact common in the opioid modeling literature, e.g., Chen et al. [2019], Linas et al. [2021].

Another line of work involves statistical learning approaches. Cooper et al. [2020] modeled the OOD growth using a polynomial regression model with time as the only covariate. Young et al. [2018] and Campo et al. [2020] tested several parametric and non-parametric statistical models on state and county level for monthly and yearly OOD prediction and found that web search data could be an important feature to model OODs. Theses models seem to be promising; however, their performances are largely affected by input features. Moreover, compared to our proposed method, these models may be unable to capture the hidden system-wide dynamics of OODs, which lead to the non-stationary space-time dependency among OODs. Moreover, both Young et al. [2018] and Campo et al. [2020] highlighted the

privacy concerns and regional and temporal variation of certain spatial covariates, such as web search data, leading to additional burdens for their practical usage.

Point Process Models with Excitation Structure. One of the important building blocks of STEMMED is the point process with an excitation structure. These models capture the interactions among a class of event streams and attempt to extract hidden information, termed *triggering effects*, between individual events, which are usually contaminated or lost during data compression or aggregation. Specifically, for event counting processes, these models jointly capture a baseline event rate, independent of the historical events, and total triggering effects, boosted by past events. Due to the rapid development of information technology that allows higher precision and granularity for data collection, point process models with distinctive excitation structures have been applied to various domains, including seismology, criminology, and epidemiology [Ogata, 1988, Mohler et al., 2011, Chiang et al., 2022]. We refer interested readers to Hawkes [1971a,b], Daley et al. [2003], and Reinhart [2018] for comprehensive reviews on this topic.

For a system of processes, mutually exciting point processes (MEPP) can be built to capture the triggering effects from other processes, in addition to itself. Researchers have successfully applied MEPP to study interactions between multiple event streams, such as advertisement clicking and purchases in online shopping investor sentiments, market returns, and invasive species pre- and post- intervention measures [Xu et al., 2014, Yang et al., 2018, Gupta et al., 2018]. However, classical MEPPs assume that the network between the member processes is directed with constant weights, which leads to an undesirably large incidence matrix and the incapability of capturing any change in these links. To model a dynamic network structure, Miscouridou et al. [2018] formulated the connections using completely random measures that promote model sparsity. Although it has a relatively small parameter space, this model requires users to fine-tune many hyper-parameters. On the other hand, Sanna Passino and Heard [2021] modeled each unit in the network with two excitation components based on events from the connected units and an added excitation structure for every connected units. This modeling approach avoids the need of tuning hyper-parameters, but leads to a large parameter space. Nevertheless, this parameter space can be searched over efficiently if a certain type of excitation structure is imposed.

Similar to MEPPs, STEMMED is equipped with directed arcs between point processes, each of which models a unique community-cause-of-death OOD event stream. Then, we use a data-driven semi-parametric form to replace the incidence matrix usually seen in standard MEPPs to model the dynamic links between the event streams while relieving computational burdens.

1.2 Contribution

Our contributions are summarized as follows.

1. For the applied point process community, we develop a novel data-driven approach for learning point process models with a dynamic network structure, wherein the baseline rate and the individual triggering effects are both modulated by a combination of static and dynamic regressors and the dynamic connections are highly contextualized. Without adding hyper-parameters or imposing certain structure to the model, STEMMED reduces the parameter space from polynomial to linear, allowing for efficient learning of the dynamic links between community-cause-of-death event streams.

2. Within substance use research community, we are among the first to address complicated global and local system-wide dynamics with one single model, STEMMED, and quantify the long-existing phenomenon of space-time clustered OOD events via triggering effects.

3. For public health practitioners, STEMMED provides a highly interpretable functional structure that works simultaneously at various community-levels, allowing for a timely and accurate estimate and system diagnosis of future OOD trends based only on available data and simple local operations and maintenance.

The remainder of this paper is structured as follows. In Section 2, we describe each component of STEMMED, including the baseline event rates, the dynamic network connections between unique community-drug event streams, and the individual triggering effect of each OOD event. We also characterize the structure of STEMMED, which leads to an efficient node-by-node model-fitting procedure. In Section 3, we use simulation to analyze how well our model-fitting procedure can recover known model parameters. Next, in Section 4, we outline an online cooperative forecasting strategy using STEMMED. Finally, we present and discuss a case study based on OOD forecasting in Massachusetts in Section 5 and provide concluding remarks in Section 6. All proofs and additional results for the case study are relegated to the online supplementary material.

2 Self/Mutually Exciting Point Process Models and STEMMED

Here, we briefly review preliminary notation for point process models with an excitation structure. We then introduce our Spatio-TEMporal Mutually Exciting point process with Dynamic network (STEMMED) and propose an efficient learning algorithm, which is the key to the localization of STEMMED.

2.1 Preliminaries on Point Processes

A point process can be viewed as a set of random vectors whose realizations form a sequence of events: $\boldsymbol{x}_1, \boldsymbol{x}_2, ...$ where each event $\boldsymbol{x} = (t_{\boldsymbol{x}}, \boldsymbol{m}_{\boldsymbol{x}})$ is described by an event time $t_{\boldsymbol{x}} \in \mathbb{R}^+$ and mark $\boldsymbol{m}_{\boldsymbol{x}} \in \mathcal{M}$. The set $\mathcal{M}$ represents a *marked space* which contains all the information of an event other than time. In general, one can take $\mathcal{M} \subset \mathbb{R}^p$ to represent the numerical encoding of additional event information, such as location, drug type, and decedent characteristics. For notational convenience, we define the set $\mathcal{X} = \mathbb{R}^+ \times \mathcal{M}$.

For any time $t > 0$, we define the history of events $\mathcal{D}^{(t)} := \{\boldsymbol{x} \in \mathcal{X} : t_{\boldsymbol{x}} < t\}$ as the set of all information about the process *right before* t. Then, we let the counting measure defined on $\mathcal{X}$ be $N_{\mathcal{S}} = |\mathcal{D}^{(T)} \cap \mathcal{S}|$, for any time horizon $T > 0$ and any measurable set $\mathcal{S} \subset \mathcal{X}$. For a function $f : \mathcal{X} \to \mathbb{R}$, the integral with respect to the counting measure $N_{\mathcal{S}}$ can be defined as:

$$\int_{\mathcal{S}} f(\boldsymbol{x}) dN_{\boldsymbol{x}} = \sum_{\boldsymbol{x} \in N_{\mathcal{S}}} f(\boldsymbol{x}). \tag{1}$$

Importantly, a point process can be characterized by its *conditional intensity function* (CIF) under history $\mathcal{D}^{(t_{\boldsymbol{x}})}$, defined as:

$$\lambda(\boldsymbol{x} \mid \mathcal{D}^{(t_{\boldsymbol{x}})}) = \mathbb{E}(dN_{\boldsymbol{x}} \mid \mathcal{D}^{(t_{\boldsymbol{x}})})/d\boldsymbol{x}. \tag{2}$$

In simple words, the CIF represents the *conditional probability* of observing a particular realization at $\boldsymbol{x} \in \mathcal{X}$, given all the observed points up to time $t_{\boldsymbol{x}}$. It is common to express $\lambda(\boldsymbol{x} \mid \mathcal{D}^{(t_{\boldsymbol{x}})})$ as $\lambda(\boldsymbol{x})$ when there is no confusion with the history on which the point process depends.

2.2 System of Point Processes with Excitation Structure

The mutually-exciting point process (MEPP), introduced by Hawkes [1971a], is a special type of point process that is especially relevant for modeling systems of processes wherein events from one node (a member process) in a network can influence future events in other nodes within the network. Specifically, the CIF of a node u in MEPP is controlled by two components: the baseline event rate, which is independent of past events, and a total triggering effect, which is collected from positive influence of every past event from any node in the network, including the node u itself. Suppose that an MEPP system has M nodes, which form a fully connected and directed network. Then, the node u in the MEPP has the following CIF:

$$\lambda_u(t) = \mu_u + \sum_{v \in [M]} A_u^v \sum_{\boldsymbol{x} \in \mathcal{D}_v^{(t)}} \kappa_{uv}(t - t_{\boldsymbol{x}}), \tag{3}$$

where $\mu_u \geq 0$ is the constant baseline event rate for the node u, $A_u^v \geq 0$ is a constant that controls the magnitude of the triggering effects from node v to node u, $\mathcal{D}_v^{(t)}$ is the history of events up to time t at node v, and $\kappa_{uv} \geq 0$ is a kernel that specifies the influence of a past event from node v to node u. Usually, $\kappa_{uv}(\cdot)$ is assumed to be shift-invariant, meaning that $\kappa_{uv}(t_1) = \kappa_{uv}(t_2)$ if $t_1 = t_2$. Moreover, due to its analytical tractability, $\kappa_{uv}(t)$ is commonly chosen to be the exponential kernel depending only on node u: $\kappa_{uv}(t') = e^{-\beta_u t'}$ with $\beta_u > 0$.

2.3 Spatio-Temporal Mutually Exciting Point Process with Dynamic Network

We now detail the formulation for STEMMED. Let I and S be the index sets for local communities and underlying causes of death (i.e., by specific drug classes) for OODs, respectively. Then, similar to MEPP, we define STEMMED by a set of nodes representing all community-drug OOD pairs $I \times S$, and arcs, representing the interactions between the nodes. To model the dynamic network arcs and the personalized (i.e., decedent-specific) influence, we extend the basic MEPP form (3) and formulate each event stream at node $\boldsymbol{u} \in I \times S$ as:

$$\lambda_{\boldsymbol{u}}(t) = \mu_{\boldsymbol{u}}(t) + \sum_{\boldsymbol{v} \in I \times S} A_{\boldsymbol{u}}^{\boldsymbol{v}}(t) \sum_{\boldsymbol{x} \in \mathcal{D}_v^{(t)}} \kappa_{\boldsymbol{u}\boldsymbol{x}}(t - t_{\boldsymbol{x}}), \tag{4}$$

where $\mu_{\boldsymbol{u}}(t) \geq 0$ is the background event rate at time t, $A_{\boldsymbol{u}}^{\boldsymbol{v}}(t) \geq 0$ dynamically controls the magnitude of influences from events occurred at node $\boldsymbol{v}$ to node $\boldsymbol{u}$, $\kappa_{\boldsymbol{x}\boldsymbol{u}}(t - t_{\boldsymbol{x}}) \geq 0$ quantifies the personalized triggering effect from the past event $\boldsymbol{x}$ to node $\boldsymbol{u}$ at time t.

Intuitively, each stream $\lambda_{\boldsymbol{u}}(t)$ consists of two major components: (1) a time-varying expected event rate that is unaffected by the triggering effects, and (2) a total triggering effect, which is a sum of the effects from *every* past event in the system. Notably, unlike MEPP, STEMMED captures the subtle differences in the triggering effects of the events via the personalized temporal kernel $\kappa_{\boldsymbol{xu}}$. These personalized triggering effects are allowed to be further amplified or attenuated over time as captured by the dynamic network $A_{\boldsymbol{u}}^{\boldsymbol{v}}(t)$.

Dynamic Baseline Event Rate. We consider a practical setting where *nodal-information*, i.e., spatial covariates determining the baseline event rate, are updated in discrete times and possibly asynchronously. For example, one can consider the US Census reports and information of state-wide programs for opioid use disorder treatment. While the former could be released annually, the latter may be published irregularly. Now, assuming p-dimensional nodal-information, we model the baseline event rate $\mu(t)$ in a log-linear form, as often used for point-process-type public health surveillance models [Meyer et al., 2012, Chiang et al., 2022]:

$$\mu_{\boldsymbol{u}}(t) := \gamma_{\boldsymbol{u}} \exp\{\boldsymbol{\beta}_{\boldsymbol{u}}^{\top} \boldsymbol{y}_{\boldsymbol{u}t}\}, \tag{5}$$

where $\gamma_{\boldsymbol{u}} \in \mathbb{R}^+$ controls the magnitude, $\boldsymbol{\beta}_{\boldsymbol{u}} \in \mathbb{R}^p$ is the regression parameter corresponding to the last update of nodal information $\boldsymbol{y}_{\boldsymbol{u}t}$, e.g., the census reports and the treatment program information, *prior* to time t.

Personalized Triggering Effects. To personalize the effect from each OOD incidence, we consider a general case wherein individual features and event times are both available. We define the personalized temporal kernel $\kappa_{\boldsymbol{xu}}$ via a product of a *temporal effect* $\kappa_{\boldsymbol{u}}$ and an *individual effect magnitude controller* $\eta_{\boldsymbol{ux}}$:

$$\kappa_{\boldsymbol{xu}}(t - t_{\boldsymbol{x}}) = \eta_{\boldsymbol{ux}} \kappa_{\boldsymbol{u}}(t - t_{\boldsymbol{x}}), \tag{6}$$

where the temporal effect $\kappa_{\boldsymbol{u}}(t') > 0$ is the exponential kernel adopted from standard SEPPs and MEPPs. We then define the individual effect magnitude controller $\eta_{\boldsymbol{ux}} : \mathbb{R}^q \to \mathbb{R}^+$ with a log-linear form, common for personalized effects [Meyer et al., 2012, Chiang et al., 2022]:

$$\eta_{\boldsymbol{ux}} = \exp\{\boldsymbol{\omega}_{\boldsymbol{u}}^{\top} \boldsymbol{m}_{\boldsymbol{x}}\}, \tag{7}$$

where $\boldsymbol{m}_{\boldsymbol{x}}$ denotes the $q-$dimensional feature vector of $\boldsymbol{x}$ in addition to event time, e.g., socioeconomic status and personal medical history, and $\boldsymbol{\omega}_{\boldsymbol{u}} \in \mathbb{R}^q$ are the coefficients associated with these features.

Dynamic Connections between Event Streams. To capture the dynamic weights on the network structure in STEMMED, we model the arcs $A_{\boldsymbol{u}}^{\boldsymbol{v}}(t)$ as a product of a *discretized spatial effects* and a *social connectivity*. We model the dynamic links between the nodes in STEMMED:

$$A_{\boldsymbol{u}}^{\boldsymbol{v}}(t) := \alpha_{\boldsymbol{u}} g_{\boldsymbol{u}}^{\boldsymbol{v}} \theta_{\boldsymbol{u}}^{\boldsymbol{v}}(t), \tag{8}$$

where $\alpha_{\boldsymbol{u}} \geq 0$ is a normalizing constant, $g_{\boldsymbol{u}}^{\boldsymbol{v}} > 0$ is the discretized spatial effects, and $\theta_{\boldsymbol{u}}^{\boldsymbol{v}}(t) \in [0, 1]$ is the social connectivity of the causes of deaths represented by node $\boldsymbol{u}$ and $\boldsymbol{v}$.

Let (i, s) and (j, s') be the community-cause-of-death pair represented by nodes u and v, respectively. In our formulation, $g_{\boldsymbol{u}}^{\boldsymbol{v}}$ captures the spatial effects between the communities i, j and is defined as: $g_{\boldsymbol{u}}^{\boldsymbol{v}} = \exp\{-\delta_{\boldsymbol{u}g}\texttt{dist}_{ij}\}$, where $\delta_{\boldsymbol{u}g}$ is a non-negative parameter and $\texttt{dist}_{ij} \geq 0$ represents the distance between community i and j. Then, we estimate $\theta_{\boldsymbol{u}}^{\boldsymbol{v}}(t)$ with the percentage of OOD events at community i, j that involved both drugs s and s', prior to time t.

By our definition of $A_{\boldsymbol{u}}^{\boldsymbol{v}}(t)$, STEMMED naturally admits a changing network structure within STEMMED, with the added benefit of reducing the number of parameters to $2|I \times S|$ compared to $|I \times S|^2$ of the static network in a standard MEPP.

2.4 Parameter Estimation

Let T denote the last observed event time, and recall that $\mathcal{D}^{(T)}$ represents the history of all events up to time T. Then, the parameters in STEMMED can be solved using Maximum Likelihood Estimation (MLE), corresponding to the following optimization problem:

$$\begin{aligned}
\hat{\Theta}_{MLE} &= \underset{\Theta}{\operatorname{argmax}} \ L(\Theta; \mathcal{D}) \\
&= \underset{\Theta}{\operatorname{argmax}} \prod_{\boldsymbol{u} \in I \times S} \prod_{t \in \{t_{\boldsymbol{x}} : \boldsymbol{x} \in \mathcal{D}_{\boldsymbol{u}}^{(T_{\boldsymbol{u}})}\}} \lambda_{\boldsymbol{u}}(t) \exp\left(-\int_0^{T_{\boldsymbol{u}}} \lambda_{\boldsymbol{u}}(z) dz\right),
\end{aligned} \tag{9}$$

where Θ denotes the parameter set in STEMMED, L represents the likelihood of STEMMED given history $\mathcal{D}$ that combines the history on every node $D_{\boldsymbol{u}}^{(T_{\boldsymbol{u}})}$ where $T_{\boldsymbol{u}}$ is the last observed event time at the node $\boldsymbol{u}$. However, (9) requires solving $(p + q + |I \times S| + 5)^2$ parameters simultaneously, which may be undesirable both from computational and practical viewpoints. In the following proposition, we alleviate this issue by decomposing (9) node-by-node, which enables learning $(p + q + |I \times S| + 5)$ parameters $|I \times S|$ times.

Proposition 2.1 *Every node in STEMMED can be learned separately, via the following log-likelihood function:*

$$\ell_{\boldsymbol{u}}\left(\Theta_{\boldsymbol{u}}; \mathcal{D}_{\boldsymbol{u}}^{(T_{\boldsymbol{u}})}\right) = \sum_{t \in \left\{t_{\boldsymbol{x}} : \boldsymbol{x} \in \mathcal{D}_{\boldsymbol{u}}^{(T_{\boldsymbol{u}})}\right\}} \log \lambda_{\boldsymbol{u}}(t) - \int_0^{T_{\boldsymbol{u}}} \lambda_{\boldsymbol{u}}(z) dz, \tag{10}$$

where $\lambda_{\boldsymbol{u}}(t)$ satisfies $(4) - (8)$.

The decomposition described in Proposition 2.1 suggests a node-by-node model-fitting procedure and shows that STEMMED can be estimated efficiently via distributed computing. Moreover, this decomposition property is the key to designing a practical data sharing and cooperation framework between different communities or agencies (see Section 4). Note that the first term in (10) depends on the past event times and can be easily computed by plugging the event times into (4). In contrast, the second term is a definite integral of (4), which depends on the data-generating processes of the local information as well as the event features. In our implementation of this MLE, we assume that these data-generating processes are left-continuous step functions where the discontinuities coincide with event times. This assumption has been widely adopted, explicitly or implicitly, for point process models involving spatial covariates and individual-level features [Meyer et al., 2012, Chiang et al., 2022] and allows us to easily compute the integral in (10). With this assumption and the decomposition from Proposition 2.1, we solve this MLE problem with the gradient descent algorithm, which is commonly used for sophisticated point process models [Ogata, 1988, Dong et al., 2021, Sanna Passino and Heard, 2021]. As (10) is non-concave, this method only finds local optimal solutions. Consequently, we use the following simulation study to evaluate this fitting procedure.

3 Simulation Analysis

In this section, we use simulation to assess how well our MLE procedure recovers the parameters of a known STEMMED model. To conduct this analysis, we simulated multiple data sets with a STEMMED-based data generating process (see Algorithm 2 in the online supplementary material). The gradient descent algorithm is then used to recover the parameters using the localized MLE (as presented in (10)). Each simulated data set corresponds to a STEMMED model with the same duration but different size. Specifically, we set the duration of the simulation to $T = 101$ and considered $N = 1, 4, 25$, and 60 nodes. For each node, we randomly selected the parameters from uniform distributions. The parameters were determined using: $\gamma \sim Unif(0, 1)$, $\beta \sim Unif(0, 1)$, $\alpha \sim Unif(1, 2)$, $\delta_g \sim Unif(6, 18)$, $\omega \sim Unif(0, 1)$, and $\delta_k \sim Unif(10, 30)$.

Since STEMMED can be learned node-by-node, as suggested in Proposition 2.1, we focused on learning one of the nodes for each dataset. To perform a fair comparison across experiments, we set the same ground truth values (GT) for the node of interest and sampled initial parameter values from the same distributions described above. We learned these nodes with cut-offs at $t = 50$ and 100, and repeated the process 100 times to construct an empirical confidence interval (CI) for the estimated parameters (EST).

Results of this analysis are summarized in Table 1. While all the mean estimated values of the parameters are very close to the ground truth parameter values, both the size of the network and the length of the training periods affect the outcomes. Specifically, the scenarios $(N, t) \in \{(1, 100), (4, 100)\}$ yield most of the best mean estimates, which are bolded in Table 1. This observation suggests that it can be easier for STEMMED to recover parameters under small networks and long training periods, compared to large networks and short training durations. In contrast, the width of the CIs were affected less by the size of the model and the training period. Although longer training periods slightly shorten the CIs, this effect was not found for node numbers. We note that wide confidence interval suggests the need of high quality initial parameter values.

4 Online Forecasting using STEMMED

In this section, we detail the online prediction strategy with STEMMED, under the context of OOD surveillance. First, we present an online OOD prediction framework based on STEMMED. We then outline a policy for interagency cooperation between local public health departments. Critically, we show that with a mild add-on to this policy, the STEMMED-based forecasting system is asymptotically robust to human error.

Table 1: STEMMED's model coefficients along with **95%** empirical confidence intervals. Best mean estimates for each parameters are marked bold.

(N,t)	γ	β	α	δ_g	ω	δ_k
GT	–	**0.77**	**0.8**	**1.45**	**8.82**	**0.85**	**14.66**
EST						
$(1, 50)$	0.74 (0, 1.31)	0.77 (0.08, 1.39)	1.4 (0.91, 1.86)	9.18 (6.35, 11.96)	0.78 (0.34, 1.26)	**14.72** (10.43, 19.65)
$(1, 100)$	**0.77** (0, 1.26)	0.84 (0.07, 1.28)	**1.45** (0.98, 1.91)	9.05 (6.35, 11.83)	**0.79** (0.39, 1.3)	14.52 (9.97, 19.52)
$(4, 50)$	0.71 (0, 1.3)	0.74 (0.06, 1.38)	1.38 (0.89, 1.84)	8.71 (6.08, 11.69)	0.77 (0.32, 1.23)	14.74 (10.46, 19.67)
$(4, 100)$	0.75 (0, 1.24)	0.81 (0.08, 1.25)	1.44 (0.97, 1.91)	**8.91** (6, 11.5)	0.78 (0.38, 1.3)	14.53 (9.98, 19.52)
$(25, 50)$	0.7 (0, 1.28)	0.73 (0.09, 1.24)	1.37 (0.88, 1.84)	8.72 (6.09, 11.7)	0.76 (0.31, 1.23)	14.76 (10.47, 19.69)
$(25, 100)$	0.74 (0, 1.23)	0.81 (0.13, 1.3)	1.43 (0.97, 1.9)	8.92 (6.01, 11.51)	0.76 (0.37, 1.29)	14.54 (9.99, 19.53)
$(60, 50)$	0.7 (0, 1.28)	0.73 (0.1, 1.37)	1.36 (0.88, 1.82)	8.93 (6.1, 11.71)	0.75 (0.3, 1.22)	14.76 (10.48, 19.69)
$(60, 100)$	0.73 (0, 1.22)	**0.8** (0.07, 1.23)	1.43 (0.96, 1.89)	8.73 (6.03, 11.52)	0.76 (0.37, 1.28)	14.55 (10, 19.54)

Algorithm 1 Multi-Period Prediction using STEMMED

Input: $t, \mathcal{D}^{(t)}, \{\lambda_{\boldsymbol{u}}(t) \mid \boldsymbol{u} \in I \times S\}, A, T$
Output: $\mathcal{D}^{(T)}$
1: **while** $t \leq T$ **do**
2:      $t^{\text{new}} \leftarrow t + A$
3:      **for** $\boldsymbol{u} \in I \times S$ **do**
4:          $n \leftarrow$ Sample from $Poisson(\int_t^{t^{\text{new}}} \lambda_{\boldsymbol{u}}(\tau)d\tau)$
5:          **for** $n_i = 1 \ldots n$ **do**
6:              $\hat{\boldsymbol{m}} \leftarrow$ Sample from $f_{\boldsymbol{u}}(\boldsymbol{m}|\mathcal{D}_{\boldsymbol{u}}^{(t)})$
7:              $\boldsymbol{x}_{n_i}^{\text{new}} \leftarrow (t^{\text{new}}, \hat{\boldsymbol{m}})$
8:              $\mathcal{D}^{(t)} \leftarrow \mathcal{D}^{(t)} \bigcup \{\boldsymbol{x}_{n_i}^{\text{new}}\}$
9:          **end for**
10:      **end for**
11:      $t \leftarrow t^{\text{new}}$
12: **end while**

4.1 Cooperative Multi-Period Prediction with STEMMED

One of the most important tasks for STEMMED is to forecast the OOD progression multiple time periods into the future to prepare for appropriate interventions, including medical, educational, and legal resource allocation. Typically, the forecasts from point process models can be done by Ogata's modified thinning algorithm [Ogata, 1981], whose main idea is to sample the next-arrival times from an Exponential distribution with CIF $\lambda_{\boldsymbol{u}}(t)$. This approach, however, is developed on continuous time and is computationally unattractive for large models, which may be less practical for public health surveillance. Moreover, STEMMED requires information beyond event times, such as spatial covariates and patient-level features, as shown in (5) and (7). To address both issues, we develop Algorithm 1 based on a common point process marginalization approach to forecast OOD trends on a discretized time space [Chiang et al., 2022, Dong et al., 2021]. Intuitively, for each node in STEMMED, we fix future spatial covariates to the last observed values and sample the amount of future events n from a Poisson distribution whose rate parameter is the integral of $\lambda_{\boldsymbol{u}}(t)$ evaluated over the time interval of interest. Then, we sample event features from its conditional distribution $f_{\boldsymbol{u}}(\boldsymbol{m}|\mathcal{D}_{\boldsymbol{u}}^{(t)})$, estimated from the shared database $\mathcal{D}$. The sampled data are then added to the database to facilitate prediction for other nodes in the next timestamps.

4.2 A Contextual Online Cooperative Forecasting Framework

As the OOD trends have been constantly evolving, it is of practical interest to update STEMMED to capture any emerging trends to improve its forecasting accuracy. However, although a shared database between local communities is realistic [Lin et al., 2019, Jones et al., 2019], it may be challenging for the local public health agencies to record every event and update STEMMED whenever a death certificate is received. In fact, the model updating and data-sharing could be more practical if staff are allowed to process the data and update the database on a regular basis, e.g., weekly or monthly.

We, therefore, propose an online data-sharing and cooperative forecasting framework based on STEMMED (See Algorithm 3 in the online supplementary material). In simple words, we assume that every local community in STEMMED's network updates the local model regularly, e.g., quarterly, semi-annually, or annually. Between these

model updates, local communities upload OOD data, on a weekly or monthly basis, to the shared database and then update their long-term forecasts. We note that the predictive performance of the proposed framework will depend on the reported data; therefore, it is important for STEMMED to limit the impacts of any operational errors, e.g., missing and/or inaccurate records, that reside in the shared database $\mathcal{D}$. In the following result, we establish that our proposed STEMMED-based online cooperative forecasting framework has this property.

Theorem 4.1 (Robustness of STEMMED-based Multi-Period Prediction) *Let $\mathcal{D}_1^{(0,t)}$, and $\mathcal{D}_2^{(0,t)}$ be two databases shared among the local communities, with data collected between time 0 and t. Suppose that both datasets are finite, i.e., for any $\tau > 0$, $|\mathcal{D}_1^{(0,\tau)}| < \infty$ and $|\mathcal{D}_2^{(0,\tau)}| < \infty$, and that $\mathcal{D}_1^{(0,\infty)}$ differs from $\mathcal{D}_2^{(0,\infty)}$ only between time interval (t, T) with $T > t \geq 0$. If $\lambda_{\boldsymbol{u}}^{[1]}$ and $\lambda_{\boldsymbol{u}}^{[2]}$ were estimated with $\mathcal{D}_1^{(0,\infty)}$ and $\mathcal{D}_2^{(0,\infty)}$ at time t, respectively, then,*

$$|\lambda_{\boldsymbol{u}}^{[1]}\big(\tau \mid \mathcal{D}_1^{(0,\infty)}\big) - \lambda_{\boldsymbol{u}}^{[2]}\big(\tau \mid \mathcal{D}_2^{(0,\infty)}\big)| \to 0 \ as \ \tau \to \infty. \tag{11}$$

Additionally, if $\mathcal{D}_1^{(0,\infty)}$ differs from $\mathcal{D}_2^{(0,\infty)}$ only for node $\boldsymbol{v} \neq \boldsymbol{u}$, then,

$$|\lambda_{\boldsymbol{u}}^{[1]}\big(\tau \mid \mathcal{D}_1^{(0,\infty)}\big) - \lambda_{\boldsymbol{u}}^{[2]}\big(\tau \mid \mathcal{D}_2^{(0,\infty)}\big)| \to 0 \ as \ \mathtt{dist}_{ij} \to \infty, \tag{12}$$

where i, j denote the local communities represented by the nodes $\boldsymbol{u}$ and $\boldsymbol{v}$, respectively.

Intuitively, Theorem 4.1 states that a learned STEMMED's predictive capability is asymptotically, "immune" to the differences in the database in the long-run and/or in a large network with wide spatial coverage. In the following, we establish that, with mild conditions, predictions made by the STEMMED-based online cooperative forecasting framework are robust to operational errors.

Corollary 4.1 (Robustness of STEMMED-based Online Forecasting) *Suppose that the local communities follow the STEMMED-based cooperative online forecasting framework and that the shared database $\mathcal{D}$ is corrected before updating the local STEMMED models. Then, the predictions made by the framework are robust to any operations error occuring to $\mathcal{D}$ between the model updates.*

Conceptually, Theorem 4.1 and Corollary 4.1 imply that the effects of operational errors could be limited to a small space-time range. Importantly, these results provide confidence for the use of the STEMMED-based cooperative forecasting system. We analyze the forecasting performance numerically of the STEMMED-based online cooperative forecasting framework in Section 5.3.

5 Case Study: Opioid Overdose Deaths in Massachusetts

In this section, we present a case study on the opioid crisis in Massachusetts (MA), USA. Firstly, we introduce our dataset, pre-processing step, and the setup for STEMMED and investigate the dynamic interactions between community-drug pairs in MA. Then, for each community-drug pairs, we compare the STEMMED-based online cooperative forecasting framework, introduced in Section 4.2, with several well-established forecasting models for short- and long-term predictions of OOD trends.

5.1 Data Overview and Preprocessing

We obtained individual-level death records ranging from January 1, 2015 to July 31, 2021, from the Massachusetts Registry of Vital Records and Statistics. We used International Classification of Diseases, Tenth Revision, Clinical Modification (ICD-10-CM) codes to identify the five underlying causes of death related to opioid-overdose [Ahmad et al., 2022]: T40.1 (Heroin), T40.2 (prescription opioids), T40.3 (Methadone), T40.4 (Fentanyl and its derivatives), and T40.6 (unspecified narcotics). In addition to the underlying causes of death, this dataset contains a subset of information appearing on decedents' death certificates, including location and time of death and other individual-level socioeconomic information such as age, gender, and race. The summary of this dataset is in Table 3.

Additionally, we obtained county-level annual census reports ranging from 2014 to 2021 from the United States Census Bureau. These data contain local socioeconomic features such as population, poverty level, and others. We further extracted opioid treatment programs directory from the Substance Abuse and Mental Health Services Administration (SAMHSA) database, which lists the name, address, and certification received date of the opioid treatment programs in MA.

To construct STEMMED, we considered nine counties in MA ($|I| = 9$) where most (97%) OODs occurred, namely, Middlesex, Suffolk, Worcester, Essex, Bristol, Hampden, Plymouth, Norfolk, and Barnstable, along with all opioid-related causes of death ($|S| = 5$). For *nodal spatial covariates*, we extracted information that may not be obtained from

Table 2: STEMMED's model coefficients along with **2.5**th and **97.5**th percentiles.

Parameters	coef	(95% CI)
Baseline (Spatial Covariates)		
$\gamma_{\boldsymbol{u}}$	0.372	$(0.074, 0.8474)$
Population/Million	0.615	$(0.054, 1.6)$
Poverty Rate	0.341	$(0.008, 0.93)$
Treatment Program Coverage	0.573	$(0.139, 0.987)$
Network Connection		
$\alpha_{\boldsymbol{u}}$	38.716	$(5.442, 58.762)$
$\delta_{\boldsymbol{ug}}$	5.469	$(0.649, 8.879)$
Individual Influence (Event Features)		
Age	0.181	$(0.034, 0.405)$
Male	0.568	$(0.097, 1.046)$
White, non-Hispanic	0.615	$(0.094, 1.377)$
Hispanic	0.48	$(0.029, 0.955)$
Black, non-Hispanic	0.376	$(0.031, 0.66)$
Asian, non-Hispanic	0.198	$(0.018, 0.495)$
Poly-Substance Involvement	0.567	$(0.053, 1.072)$
Temporal Effect		
$\delta_{\boldsymbol{uk}}$	8.002	$(6.91, 8.77)$

death certificates, namely population per million, poverty rate, and the coverage of rehab programs, which is defined by the number of OOD events related to cause of death s per treatment program in county i. While the population and poverty rate were updated annually, treatment program information were assumed to be released monthly. For *event-features*, we selected age, sex, race and ethnicity, and poly-substance involvement, which have been shown to be highly associated with OODs [Scholl et al., 2019]. Furthermore, we applied one-hot encoding for sex and ethnicity and race and kept the new features except for the last generated features to avoid multicollinearity. The resulting features are: Age, Male, White (non-Hispanic), Hispanic, Black (non-Hispanic), Asian (non-Hispanic), and Poly-substance Involvement.

5.2 Retrospective Analysis

We applied STEMMED to the entire dataset and discretized it on a monthly basis to facilitate analysis. To start the fitting procedure, we randomly selected the initial parameters for baseline rate μ and personalized effects $\eta_{\boldsymbol{x}}$ from $Unif(0, 1)$. We then applied grid search to set the initial values for the rest of the parameters: $\alpha_{\boldsymbol{u}} = 30$, $\delta_{\boldsymbol{uk}} = 5$, and $\delta_{\boldsymbol{ug}} = 5$.

5.2.1 Estimated parameters.

Table 2 shows the mean estimated parameters and coefficients along with their 95% CIs across STEMMED's nodes. We observed that all spatial covariates are important for STEMMED, since 0 was not contained in any 95% CIs. Moreover, Population, Poverty Rate, and Treatment Program Coverage are all positively correlated with the intensity function, meaning that the expected amount of OODs increases with these spatial covariates. However, the estimated coefficients of both population per million and poverty rate are right-skewed, indicating that these two covariates have fewer impacts in most nodes. Additionally, the lower CI of the estimated coefficients for poverty rate is close to 0, potentially indicating that Poverty Rate may have little effects for some nodes in STEMMED.

For the event features, OODs among non-Hispanic White people, in general, have higher impact (0.615) to the triggering effects, compared to the influences from OODs among Hispanic people (0.48), non-Hispanic Black people (0.376), and non-Hispanic Asian (0.198). While OODs among male decedents and decedents with poly-substance involvement have slightly fewer impacts compared to decedents who are non-Hispanic White, age has the smallest positive correlation with the triggering effects. Moreover, similar to poverty rate in the background event rate, the lower CIs of the coefficients for individual event features are close to 0. Although further analyses are needed, our results highlight the varying importance of these local spatial covariates and the individual-level features across counties and drug use patterns in MA, resonating with Pear et al. [2019]'s findings on the dynamic importance of socioeconomic factors in OODs across geographical areas.
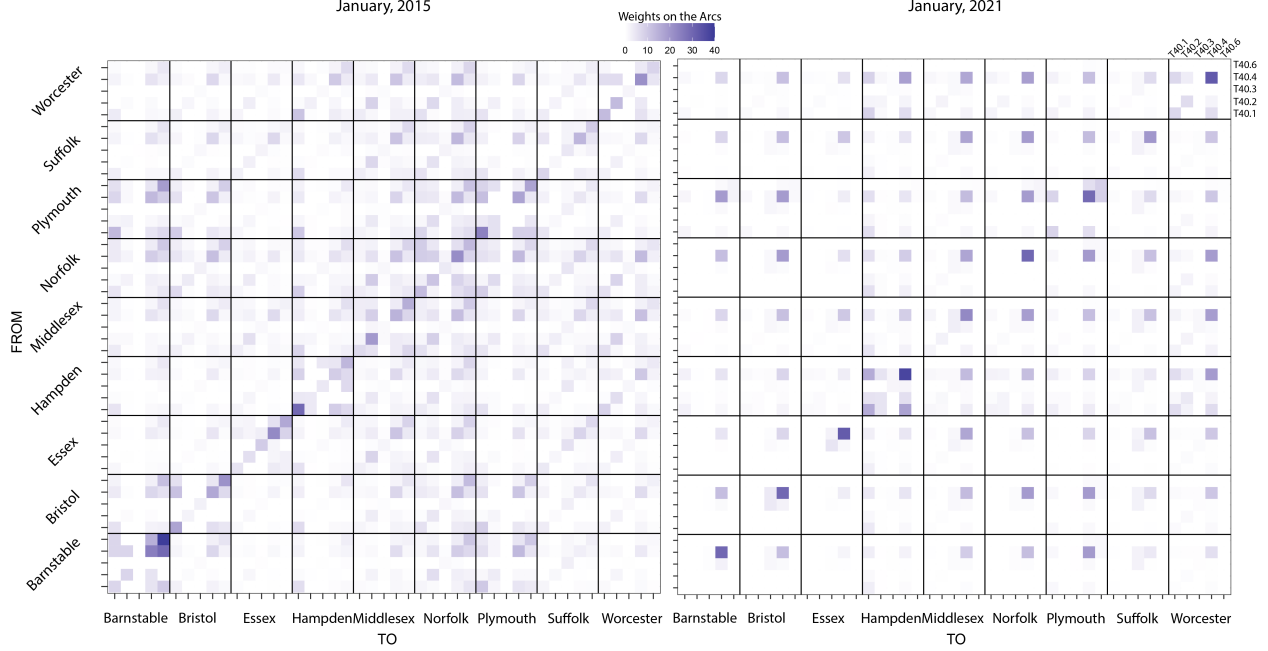
Figure 1: The network structure of STEMMED in January 2015, and January 2021.

Finally, we found that the learned temporal effects have a fast decreasing rate as δ_k centers at 8.002 with a small variation across all nodes. Although it suggests that the influence from each OOD event may not last long, the events influence the nodes differently, as admitted by the dynamic network connections and the personalized triggering effects.

5.2.2 Dynamic Network Connections in STEMMED.

Figure 1 shows the dynamic network of STEMMED in January 2015 and January 2021, respectively. We observed that the incidence matrix, representing the links between nodes, is asymmetric; however, the connections between any two nodes generally have comparable strengths. For example, while the connection from (Barnstable, T40.4) to (Barnstable, T40.6) is stronger than links from (Barnstable, T40.6) to (Barnstable, T40.4), the connections between other nodes are similar. This behavior may arise because the dynamic nature of the network comes directly from the social connectivity between drugs, which is shared by the connected nodes, with a range of $[0, 1]$, thereby making the arcs almost even weights in many cases. Overall, the connections were the strongest among the antidiagonals, i.e., upper-right to lower-left, in both matrices, meaning that the events occurring at one node tend to have the greatest influence at that node. This finding suggests that the OOD events involved in one drug are associated primarily with the same drug at the same location, rather than other drug types or different counties.

Additionally, the arcs are usually stronger between drugs, compared to connections between counties. In other words, nodes representing different counties with the same drug are considerably "closer" to each other than nodes representing the same county with different drug types. Interestingly, nodes representing T40.2 and T40.3 usually have weaker links between other nodes in STEMMED. This is probably because that the drugs represented by these two codes are primarily seen in medical uses with proper instructions and lower potency. Specifically, T40.2 mainly represents prescribed opioids and are not commonly involved in illicit drug trades in recent years as prescribers have been cautious about prescribing them due to numerous laws and initiatives following the prescription opioid wave of the opioid crisis [Volkow and Blanco, 2021]. On the other hand, T40.3 represents methadone, which is often used as an opioid agonist medication for the treatment of opioid use disorder [Volkow and Blanco, 2021]. Therefore, nodes involving T40.2 and T40.3 are naturally isolated in STEMMED's network.

Finally, as the connections between fentanyl and its analogs (T40.4) had been strengthened during the study period, the exact opposite can be found for other types of connections. This observation is in parallel with the OOD cases in MA where fentanyl-related OOD has dominated the opioid crisis in recent years [DiGennaro et al., 2021, Garcia et al., 2022]. Our findings may suggest local governments to form cross-region strategic partnerships to design overdose prevention measures based on certain drug use behaviors.
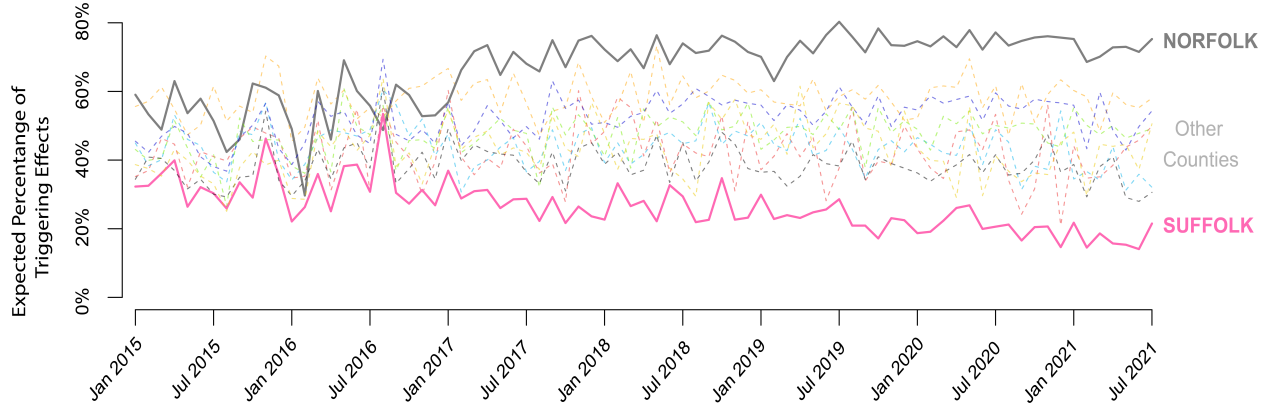
Figure 2: Percentages of expected OODs explained by triggering effects for each county, across the study period. Here we highlight counties with highest and lowest overall triggering percentage, respectively, namely, Norfolk County and Suffolk County.

5.2.3 County-Level Triggering Effects.

We calculated the proportion of expected number of OODs explained by triggering effects for each county during the study period (Figure 2). We note that this proportion of total triggering effects in STEMMED can imply the expected percentage of OODs belonging to *series of past events*, which lightly resembles "modus operandi" in crime analysis [Zhu and Xie, 2022]. In other words, by splitting the baseline event rate and total triggering effect in the expected number of OOD events, public health officials can obtain a clearer view of the system-wide dynamics, which could lead to effective regional collaborative partnerships among state public health departments.

From Figure 2, we noticed that Norfolk had suffered the most from the triggering effects, while Suffolk had been impacted by these effects the least. Although the triggering effects generally explained around $40 - 50\%$ of the expected OODs for most counties during the study period, it had been around $60 - 80\%$ for Norfolk and 30% for Suffolk. Moreover, this proportion had increased from 60% to 75% since January 2017 in Norfolk but had gradually decreased in Suffolk, from 35% to around 20%. We reiterate that this percentage represents the degree a county was influenced by other counties in MA. Consequently, these results imply that OODs in Norfolk had stronger connections with opioids in other counties, whereas OODs in Suffolk were likely to originate from Suffolk itself.

While the geographical positions of Norfolk and Suffolk may be an explanation for these results, socioeconomic disparities among these counties may also play a key role [Pear et al., 2019]. In fact, Norfolk County is located to the Southwest of the city of Boston and has had lower economic distress compared to the Suffolk County, which contains the city of Boston. Consequently, these results might potentially suggest that the influences of past OODs could "flow" from urban areas to suburbs, which resonates with findings by Cicero et al. [2014] and Althoff et al. [2020]. As such, there is a need for thorough investigations into the dynamics of drug use behaviors and, potentially, the illicit drug supply and/or prescribed medications in not only Norfolk and Suffolk but also nearby counties to design suitable cross-regional intervention measures.

We note that these insights generated by STEMMED provide a unique approach for public health surveillance. Although the analysis was county-based, local governments can further break down the results into more granular levels, e.g., zip codes or particular communities and census tracts, to obtain a clearer view of the local OOD patterns.

5.3 Online Predictive Performance of STEMMED-Based Cooperative System

To assess the predictive performance of the STEMMED-based online cooperative forecasting system, we assumed that the database $\mathcal{D}$ is updated quarterly, which is immediately followed by the updates of STEMMED. Then, these models start to make predictions for OOD trends $1, 3, 6, 9$, and 12 months into the future.

5.3.1 Model Specification for Online Forecasting.

To investigate the benefit of incorporating individual level data, community-level covariates, and the network structure for forecasting OOD trends, we included the standard self- and mutually- exciting point processes (SEPP and MEPP), the Autoregressive Integrated Moving Average model (ARIMA), and the Vector Auto-Regressive model (VAR). While
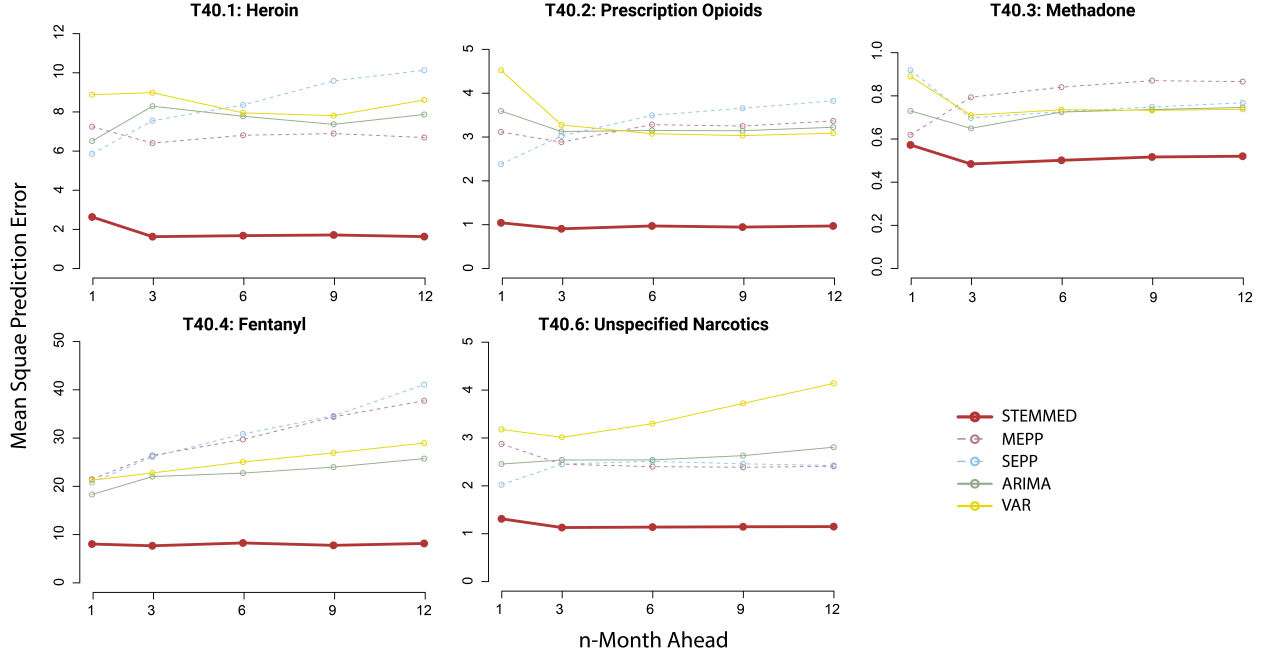
Figure 3: Mean Square Prediction Errors of the STEMMED-based cooperative Forecasting framework and the benchmarks on **1**–, **3**–, **6**–, **9**–, **12**–month ahead predictions, aggregated by underlying cause of death. Note that the scales of y-axes are different to better show the differences.

SEPP and MEPP are point process models, ARIMA and VAR are time series models frequently used to capture temporal dependency of aggregated data and to forecast future trends. Similar to MEPPs, VAR models the network connections between event streams.

As in standard SEPP and MEPP, we used constants for the baseline rates and adopted exponential kernels for the triggering effects. Also, the network connections in MEPP are constants. We then picked the order terms for ARIMA and VAR by grid search using the initial training period, which was set to the first 2 years to ensure stable estimates from these time series models. The resulting time series models were ARIMA$(1, 1, 1)$ and VAR(1). Finally, to perform a fair comparison, all models were learned with the same strategy, i.e., starting from January 1, 2017, these models were fit on each county-cause-of-death event stream on a quarterly basis with the entire historical data up to that time. Then, the fitted models made forecasts for future OOD trends. Mean Square Prediction Error (MSPE) was the main metric to measure model performance.

5.3.2 Analyzing Online Forecasting Performance of STEMMED.

We aggregated the results by underlying cause of death, shown in Figure 3. Noticeably, STEMMED outperformed all competing models in terms of prediction accuracy. Specifically, STEMMED was $70 - 72\%$ better than SEPP and MEPP and $65 - 69\%$ better than ARIMA and VAR. Furthermore, we found that STEMMED provides the greatest edge in predicting the amounts of heroin-involved OOD (T40.1), with an average of MSPE $= 1.85$. On the other hand, comparing with ARIMAs and VAR, SEPP and MEPP can yield better performance for short-term forecasts; however, their long-term MSPEs can be high when forecasting future heroin-involved OODs (T40.1) and fentanyl-involved OODs (T40.4). These observations may be due to the fact that predictive errors may last in SEPP and MEPP longer, compared to the time series models. Although ARIMA and VAR rely on their imperfect predictions to make future ones, the dependence vanishes after some periods controlled by the order terms. In contrast, standard SEPP and MEPP could reuse their predictions after longer durations, depending on the learned temporal kernel. Nevertheless, SEPP and MEPP still performed well for short-term predictions. As the quality of these two largely depend on the initial parameter values and the chosen temporal kernels, fine-tuned point process models that leverage individual event can have great potential for practical uses.

Importantly, STEMMED's MSPE, in all prediction tasks, does not increase with the forecasting horizons as much as the others. The major reason for STEMMED's outstanding performance could be the nature of the model. While STEMMED is localized via the dynamic baseline event rates with important socioeconomic factors, the design of

12

triggering effects allows STEMMED to leverage personalized influences from each OOD. Moreover, STEMMED's data-driven network connections provide a safer way to "borrow" space-time varying effects of OODs from other nodes, which is critical to model the complicated and rapidly changing opioid crisis. In other words, STEMMED's sophisticated triggering structure helps with hedging the risks of mis-specification and mis-prediction of OOD events. That said, STEMMED's capability of capturing the subtle interactions between past and future events across counties and drug-use behaviors was achieved by highly interpretable dynamic network structure, local spatial covariates, and personalized triggering effects without imposing any explicit and complicated assumptions on system-level dynamics.

6   Conclusion

In this work, we introduced a Spatio-TEMporal Mutually Exciting point process with Dynamic network structure (STEMMED) to address the needs of an accurate opioid overdose death (OOD) forecasting system that is feasible to implement locally. STEMMED quantifies the subtle connections between past and future OOD events across a wide range of local communities and drug use behaviors and can be easily decomposed node-by node, which suggests a tractable learning algorithm. Using simulation, we found that this algorithm can recover known parameters of STEMMED, especially for those with smaller number of nodes and longer study periods. Then, using STEMMED's decomposability, we designed a practical online cooperative forecasting framework that can be operated at various community levels and is robust to operational errors.

Our case study involving nine counties in Massachusetts (MA) revealed stronger connections among counties with the same drug types, comparing to that among different drug types in the same county. Additionally, Norfolk had suffered the most from past events' effects while Suffolk had been influenced by the triggering effects the least, which can inform the design of strategic partnerships between the counties in MA. Furthermore, STEMMED-based cooperative forecasting framework outperformed the other models in both short- and long-term predictions in an online forecasting, indicating its capability of capturing the intricate yet subtle connections between past and future events.

We highlight several key practical advantages of STEMMED. Firstly, both the nodal-information and the event-level features that determine a local STEMMED model can be customized to further reflect the regional variations of OOD trends and improve STEMMED's overall performance. Additionally, STEMMED's strong performance in long-term predictions is desirable for policy planning, especially under the 4 months to 2 years time lag in the current OOD reporting systems. Finally, through the inspection of the dynamic connections between community-drug pairs, the local communities participating in the cooperative framework can plan for better evidence-based collaborations to efficiently allocate medical, educational, and legal resources to combat the opioid crisis locally.

Our study has limitations. Firstly, causal relationships between the event streams may not be directly inferred from the dynamic network connections in STEMMED. Moreover, there might be difficulties for data sharing between local communities due to privacy issues. However, STEMMED does not require identifiable information such as personal medical history, which may increase governments' willingness to construct shared databases. Finally, the case study was a singe state analysis and STEMMED, as a spatio-temporal model, suffers from the so-called boundary effects; that is, the model cannot capture the effects from units outside the modeled network. Large scale analyses with many participating states may mitigate this issue.

In closing, STEMMED is a novel forecasting tool that captures the dynamic yet subtle links between past and future events of distinct types. While STEMMED was motivated by OOD prediction, its key analytical properties facilitate its application to other domains, including diseases surveillance, demand planning, crime analysis, and cybersecurity.

References

F. Ahmad, J. Cisewski, L. Rossen, and P. Sutton. Provisional drug overdose death counts. *National Center for Health Statistics*, 2022.

S. F. Altekruse, C. M. Cosgrove, W. C. Altekruse, R. A. Jenkins, and C. Blanco. Socioeconomic risk factors for fatal opioid overdoses in the united states: Findings from the mortality disparities in american communities study (mdac). *PLoS One*, 15(1):e0227966, 2020.

K. N. Althoff, K. M. Leifheit, J. N. Park, A. Chandran, and S. G. Sherman. Opioid-related overdose mortality in the era of fentanyl: monitoring a shifting epidemic by person, place, and time. *Drug and alcohol dependence*, 216:108321, 2020.

C. Bharat, M. Hickman, S. Barbieri, and L. Degenhardt. Big data and predictive modelling for the opioid crisis: existing research and future potential. *The Lancet Digital Health*, 3(6):e397–e407, 2021.

D. S. Campo, J. W. Gussler, A. Sue, P. Skums, and Y. Khudyakov. Accurate spatiotemporal mapping of drug overdose deaths by machine learning of drug-related web-searches. *Plos one*, 15(12):e0243622, 2020.

J. G. Carter, G. Mohler, and B. Ray. Spatial concentration of opioid overdose deaths in indianapolis: an application of the law of crime concentration at place to a public health epidemic. *Journal of contemporary criminal justice*, 35(2): 161–185, 2019.

Q. Chen, M. R. Larochelle, D. T. Weaver, A. P. Lietz, P. P. Mueller, S. Mercaldo, S. E. Wakeman, K. A. Freedberg, T. J. Raphel, A. B. Knudsen, et al. Prevention of prescription opioid misuse and projected overdose deaths in the united states. *JAMA network open*, 2(2):e187621–e187621, 2019.

W.-H. Chiang, X. Liu, and G. Mohler. Hawkes process modeling of covid-19 with mobility leading indicators and spatial covariates. *International journal of forecasting*, 38(2):505–520, 2022.

D. Ciccarone. The rise of illicit fentanyls, stimulants and the fourth wave of the opioid overdose crisis. *Current Opinion in Psychiatry*, 34(4):344–350, 2021.

T. J. Cicero, M. S. Ellis, H. L. Surratt, and S. P. Kurtz. The changing face of heroin use in the united states: a retrospective analysis of the past 50 years. *JAMA psychiatry*, 71(7):821–826, 2014.

R. L. Cooper, J. Thompson, R. Edgerton, J. Watson, S. A. MacMaster, M. Kalliny, M. M. Huffman, P. Juarez, P. Mathews-Juarez, M. Tabatabai, et al. Modeling dynamics of fatal opioid overdose by state and across time. *Preventive medicine reports*, 20:101184, 2020.

D. J. Daley, D. Vere-Jones, et al. *An introduction to the theory of point processes: volume I: elementary theory and methods*. Springer, 2003.

Z. F. Dembek, T. Chekol, and A. Wu. The opioid epidemic: challenge to military medicine and national security. *Military medicine*, 185(5-6):e662–e667, 2020.

C. DiGennaro, G.-G. P. Garcia, E. J. Stringfellow, S. Wakeman, and M. S. Jalali. Changes in characteristics of drug overdose death trends during the covid-19 pandemic. *International Journal of Drug Policy*, 98:103392, 2021.

Z. Dong, S. Zhu, Y. Xie, J. Mateu, and F. J. Rodríguez-Cortés. Non-stationary spatio-temporal point process modeling for high-resolution covid-19 data. *arXiv preprint arXiv:2109.09029*, 2021.

G.-G. P. Garcia, E. J. Stringfellow, C. DiGennaro, N. Poellinger, J. Wood, S. Wakeman, and M. S. Jalali. Opioid overdose decedent characteristics during covid-19. *Annals of Medicine*, 54(1):1081–1088, 2022.

A. Gupta, M. Farajtabar, B. Dilkina, and H. Zha. Discrete interventions in hawkes processes with applications in invasive species management. In *IJCAI*, pages 3385–3392, 2018.

L. Gussow. Toxicology rounds: who said the opioid crisis couldn't get any worse? *Emergency Medicine News*, 38(11): 1–29, 2016.

A. G. Hawkes. Point spectra of some mutually exciting point processes. *Journal of the Royal Statistical Society: Series B (Methodological)*, 33(3):438–443, 1971a.

A. G. Hawkes. Spectra of some self-exciting and mutually exciting point processes. *Biometrika*, 58(1):83–90, 1971b.

A. Hernandez, A. J. Branscum, J. Li, N. J. MacKinnon, A. L. Hincapie, and D. F. Cuadros. Epidemiological and geospatial profile of the prescription opioid crisis in ohio, united states. *Scientific reports*, 10(1):1–10, 2020.

J. Homer and W. Wakeland. A dynamic model of the opioid drug epidemic with implications for policy. *The American Journal of Drug and Alcohol Abuse*, 47(1):5–15, 2021.

K. Johnson, C. Jones, W. Compton, G. Baldwin, J. Fan, J. Mermin, and J. Bennett. Federal response to the opioid crisis. *Current HIV/AIDs Reports*, 15(4):293–301, 2018.

M. R. Jones, M. B. Novitch, S. Sarrafpour, K. P. Ehrhardt, B. B. Scott, V. Orhurhu, O. Viswanath, A. D. Kaye, J. Gill, and T. T. Simopoulos. Government legislation in response to the opioid epidemic. *Current Pain and Headache Reports*, 23(6):1–7, 2019.

C.-Y. Liao, G.-G. P. Garcia, C. DiGennaro, and M. S. Jalali. Racial disparities in opioid overdose deaths in massachusetts. *JAMA Network Open*, 5(4):e229081–e229081, 2022.

T. Y. Lim, E. J. Stringfellow, C. A. Stafford, C. DiGennaro, J. B. Homer, W. Wakeland, S. L. Eggers, R. Kazemi, L. Glos, E. G. Ewing, C. B. Bannister, K. Humphreys, D. C. Throckmorton, and M. S. Jalali. Modeling the evolution of the u.s. opioid crisis for national policy development. *PNAS*, 119(23), 2022.

H.-C. Lin, Z. Wang, L. Simoni-Wastila, C. Boyd, and A. Buu. Interstate data sharing of prescription drug monitoring programs and associated opioid prescriptions among patients with non-cancer chronic pain. *Preventive Medicine*, 118:59–65, 2019.

B. P. Linas, A. Savinkina, R. Madushani, J. Wang, G. E. Yazdi, A. Chatterjee, A. Y. Walley, J. R. Morgan, R. L. Epstein, S. A. Assoumou, et al. Projected estimates of opioid mortality after community-level interventions. *JAMA network open*, 4(2):e2037259–e2037259, 2021.

K. M. Lippold, C. M. Jones, E. O. Olsen, and B. P. Giroir. Racial/ethnic and age group differences in opioid and synthetic opioid–involved overdose deaths among adults aged $\geq$ 18 years in metropolitan areas—united states, 2015–2017. *Morbidity and Mortality Weekly Report*, 68(43):967, 2019.

C. L. Mattson, L. J. Tanz, K. Quinn, M. Kariisa, P. Patel, and N. L. Davis. Trends and geographic patterns in drug and synthetic opioid overdose deaths—united states, 2013–2019. *Morbidity and Mortality Weekly Report*, 70(6):202, 2021.

S. Meyer, J. Elias, and M. Höhle. A space–time conditional intensity model for invasive meningococcal disease occurrence. *Biometrics*, 68(2):607–616, 2012.

X. Miscouridou, F. Caron, and Y. W. Teh. Modelling sparsity, heterogeneity, reciprocity and community structure in temporal interaction data. *Advances in Neural Information Processing Systems*, 31, 2018.

G. O. Mohler, M. B. Short, P. J. Brantingham, F. P. Schoenberg, and G. E. Tita. Self-exciting point process modeling of crime. *Journal of the American Statistical Association*, 106(493):100–108, 2011.

National Center for Health Statistics (NCHS). Multiple cause of death 1999-2020 on cdc wonder online database, 2021. Data are compiled from data provided by the 57 vital statistics jurisdictions through the Vital Statistics Cooperative Program.

Y. Ogata. On lewis' simulation method for point processes. *IEEE transactions on information theory*, 27(1):23–31, 1981.

Y. Ogata. Statistical models for earthquake occurrences and residual analysis for point processes. *Journal of the American Statistical association*, 83(401):9–27, 1988.

V. A. Pear, W. R. Ponicki, A. Gaidus, K. M. Keyes, S. S. Martins, D. S. Fink, A. Rivera-Aguirre, P. J. Gruenewald, and M. Cerdá. Urban-rural variation in the socioeconomic determinants of opioid overdose. *Drug and alcohol dependence*, 195:66–73, 2019.

A. L. Pitt, K. Humphreys, and M. L. Brandeau. Modeling health benefits and harms of public policy responses to the us opioid epidemic. *American journal of public health*, 108(10):1394–1400, 2018.

A. Reinhart. A review of self-exciting spatio-temporal point processes and their applications. *Statistical Science*, 33(3): 299–318, 2018.

F. Sanna Passino and N. A. Heard. Mutually exciting point process graphs for modelling dynamic networks. *arXiv e-prints*, pages arXiv–2102, 2021.

L. Scholl, P. Seth, M. Kariisa, N. Wilson, and G. Baldwin. Drug and opioid-involved overdose deaths—united states, 2013–2017. *Morbidity and mortality weekly report*, 67(51-52):1419, 2019.

E. J. Stringfellow, T. Y. Lim, K. Humphreys, C. DiGennaro, C. Stafford, E. Beaulieu, J. Homer, W. Wakeland, B. Bearnot, R. K. McHugh, et al. Reducing opioid use disorder and overdose deaths in the united states: A dynamic modeling analysis. *Science advances*, 8(25):eabm8147, 2022.

N. Vadivelu, A. M. Kai, V. Kodumudi, J. Sramcik, and A. D. Kaye. The opioid crisis: a comprehensive overview. *Current pain and headache reports*, 22(3):1–6, 2018.

N. D. Volkow and C. Blanco. The changing opioid crisis: development, challenges and opportunities. *Molecular psychiatry*, 26(1):218–233, 2021.

L. Xu, J. A. Duan, and A. Whinston. Path to purchase: A mutually exciting point process model for online advertising and conversion. *Management Science*, 60(6):1392–1412, 2014.

S. Y. Yang, A. Liu, J. Chen, and A. Hawkes. Applications of a multivariate hawkes process to joint modeling of sentiment and market return events. *Quantitative finance*, 18(2):295–310, 2018.

S. D. Young, K. Zheng, L. F. Chu, and K. Humphreys. Internet searches for opioids predict future emergency department heroin admissions. *Drug and alcohol dependence*, 190:166–169, 2018.

S. Zhu and Y. Xie. Spatiotemporal-textual point processes for crime linkage detection. *The Annals of Applied Statistics*, 16(2):1151–1170, 2022.

Appendix

Proof of Proposition 2.1. By taking the logarithm of (9), we obtain the log-likelihood function of STEMMED, as the following.

$$\ell(\Theta; \mathcal{D}) = \log L(\Theta; \mathcal{D})$$

$$= \log \prod_{\boldsymbol{u} \in I \times S} \prod_{t \in \{t_{\boldsymbol{x}} : \boldsymbol{x} \in \mathcal{D}_{\boldsymbol{u}}^{(T_{\boldsymbol{u}})}\}} \lambda_{\boldsymbol{u}}(t) \exp\left\{ -\int_0^{T_{\boldsymbol{u}}} \lambda_{\boldsymbol{u}}(z) dz \right\} \tag{13}$$

$$= \sum_{\boldsymbol{u} \in I \times S} \sum_{t \in \{t_{\boldsymbol{x}} : \boldsymbol{x} \in \mathcal{D}_{\boldsymbol{u}}^{(T_{\boldsymbol{u}})}\}} \log \lambda_{\boldsymbol{u}}(t) - \int_0^{T_{\boldsymbol{u}}} \lambda_{\boldsymbol{u}}(z) dz.$$

From the definition of $\lambda_{\boldsymbol{u}}(t)$, it is clear that no parameter is shared by two nodes in STEMMED. Consequently, Θ is the Cartesian products of $\Theta_{\boldsymbol{u}}$ for all $\boldsymbol{u} \in I \times S$, where $\Theta_{\boldsymbol{u}} = (\gamma, \boldsymbol{\beta}, \delta_k, \boldsymbol{\omega}, \alpha, \delta_g)_{\boldsymbol{u}}$, as specified in (5) – (8). Hence, WLOG, we have:

$$\arg\max_{\Theta} \ell(\Theta; \mathcal{D}) = \bigcup_{\boldsymbol{u} \in I \times S} \arg\max_{\Theta_{\boldsymbol{u}}} \ell_{\boldsymbol{u}}\left(\Theta_{\boldsymbol{u}}; \mathcal{D}_{\boldsymbol{u}}^{(T_{\boldsymbol{u}})}\right), \tag{14}$$

where

$$\ell_{\boldsymbol{u}}\left(\Theta_{\boldsymbol{u}}; \mathcal{D}_{\boldsymbol{u}}^{(T_{\boldsymbol{u}})}\right) = \sum_{t \in \{t_{\boldsymbol{x}} : \boldsymbol{x} \in \mathcal{D}_{\boldsymbol{u}}^{(T_{\boldsymbol{u}})}\}} \log \lambda_{\boldsymbol{u}}(t) - \int_0^{T_{\boldsymbol{u}}} \lambda_{\boldsymbol{u}}(z) dz. \tag{15}$$

∎

Proof of Theorem 4.1. Take any arbitrary time interval $B = (t, T)$. Define $\mathcal{X}^B$ as a set containing the discrepancy between the two databases, i.e.,

$$\mathcal{X}^B := \left\{ \boldsymbol{x} \in \mathcal{D}_1^{(B)} \cup \mathcal{D}_2^{(B)} \mid \boldsymbol{x} \text{ represents the OOD event that only appears in one database} \right\}.$$

Now, we observe that $|\mathcal{X}^B| \leq |\mathcal{D}_1^{(B)} \cup \mathcal{D}_2^{(B)}| < \infty$. Hence, we have, for any $\tau > 0$,

$$|\lambda_{\boldsymbol{u}}^{[1]}(\tau) - \lambda_{\boldsymbol{u}}^{[2]}(\tau)| = \left| \mu_{\boldsymbol{u}}(\tau) + \sum_{\boldsymbol{v} \in I \times S} A_{\boldsymbol{u}}^{\boldsymbol{v}, [1]}(\tau) \sum_{\boldsymbol{x} \in \mathcal{D}_{\boldsymbol{v}, 1}^{(0, \tau)}} \eta_{\boldsymbol{u}\boldsymbol{x}}^{[1]} \kappa_{\boldsymbol{u}}^{[1]}(\tau - t_{\boldsymbol{x}}) \right.$$

$$\left. - \mu_{\boldsymbol{u}}(\tau) - \sum_{\boldsymbol{v} \in I \times S} \bar{A}_{\boldsymbol{u}}^{\boldsymbol{v}, [2]}(\tau) \sum_{\bar{\boldsymbol{x}} \in \mathcal{D}_{\boldsymbol{v}, 2}^{(0, \tau)}} \eta_{\boldsymbol{u}\boldsymbol{x}}^{[2]} \kappa_{\boldsymbol{u}}^{[2]}(\tau - t_{\boldsymbol{x}}) \right| \tag{16}$$

$$\leq K \left| \sum_{\boldsymbol{v} \in I \times S} \left(\sum_{\boldsymbol{x} \in \mathcal{D}_{\boldsymbol{v}, 1}^{(0, \tau)}} \eta_{\boldsymbol{u}\boldsymbol{x}}^{[1]} \kappa_{\boldsymbol{u}}^{[1]}(\tau - t_{\boldsymbol{x}}) - \sum_{\boldsymbol{x} \in \mathcal{D}_{\boldsymbol{v}, 2}^{(0, \tau)}} \eta_{\boldsymbol{u}\boldsymbol{x}}^{[2]} \kappa_{\boldsymbol{u}}^{[2]}(\tau - t_{\boldsymbol{x}}) \right) \right| \tag{17}$$

$$= K \left| \sum_{\boldsymbol{x} \in \mathcal{X}^B} \eta_{\boldsymbol{u}\boldsymbol{x}}^{[1]} \kappa_{\boldsymbol{u}}^{[1]}(\tau - t_{\boldsymbol{x}}) - \eta_{\boldsymbol{u}\boldsymbol{x}}^{[2]} \kappa_{\boldsymbol{u}}^{[2]}(\tau - t_{\boldsymbol{x}}) \right| \tag{18}$$

$$\leq K \sum_{\boldsymbol{x} \in \mathcal{X}^B} \left| \eta_{\boldsymbol{u}\boldsymbol{x}}^{[1]} \kappa_{\boldsymbol{u}}^{[1]}(\tau - t_{\boldsymbol{x}}) - \eta_{\boldsymbol{u}\boldsymbol{x}}^{[2]} \kappa_{\boldsymbol{u}}^{[2]}(\tau - t_{\boldsymbol{x}}) \right| \tag{19}$$

$$\leq K \sum_{\boldsymbol{x} \in \mathcal{X}^B} \left| \left(\eta_{\boldsymbol{u}\boldsymbol{x}}^{[1]} - \kappa_{\boldsymbol{u}}^{[2]}(\tau - t_{\boldsymbol{x}}) \right) \kappa_{\boldsymbol{u}}^{[1]}(\tau - t_{\boldsymbol{x}}) \right| + \left| \left(\eta_{\boldsymbol{u}\boldsymbol{x}}^{[2]} - \kappa_{\boldsymbol{u}}^{[1]}(\tau - t_{\boldsymbol{x}}) \right) \kappa_{\boldsymbol{u}}^{[2]}(\tau - t_{\boldsymbol{x}}) \right|, \tag{20}$$

where K is a large enough constant, coming from the fact the $A_{\boldsymbol{u}}^{\boldsymbol{v}}(\tau) < \infty$ for any $\tau > 0$. Now, since κ is monotone decreasing by design, both absolute terms in (20) converge to 0. Finally, $|\mathcal{X}^B| < \infty$ implies:

$$|\lambda_{\boldsymbol{u}}^{[1]}\left(\tau \mid \mathcal{D}_1^{(0, \infty)}\right) - \lambda_{\boldsymbol{u}}^{[2]}\left(\tau \mid \mathcal{D}_2^{(0, \infty)}\right)| \to 0 \text{ as } \tau \to \infty. \tag{21}$$

Note that the second part of this theorem can be proved by a similar argument, replacing the temporal kernel $\kappa_{\boldsymbol{u}}$ with the spatial kernel $g_{\boldsymbol{u}}^{\boldsymbol{v}}$. ∎

Proof of Theorem 4.1 Let $\mathcal{D}$ be the shared database among the local communities and $\bar{\mathcal{D}}$ be the correct version of $\mathcal{D}$. By our assumption, we have that $\mathcal{D}$ can only differ from $\bar{\mathcal{D}}$ during the time periods between the last model update and the next model update. Then, it follows from Theorem 4.1 that the long-term predictions made by the STEMMED-based cooperative forecasting framework are asymptotically robust to the operational errors. ∎

Computing the Log-likelihood. Proposition 2.1 shows that STEMMED can be decomposed node-by-node, which suggests a tractable learning algorithm involving likelihood function for each node (10). It is clear that the first term in the likelihood function can be obtained by plugging in the event times. In the following proposition, we present a closed-form expression of the remaining integral, under mild conditions.

Proposition 6.1 *Assume the spatial covariates are left-continuous step functions, where the discontinuities coincide with event times. Then the integral in* (10) *can be simplified to:*

$$\int_0^T \lambda_{\boldsymbol{u}}(z)dz = \sum_{h \in \{t_{\boldsymbol{y}} | \boldsymbol{y} \in \mathcal{D}\}} \left\{ \mu_{\boldsymbol{u}}(h^{-1})\Delta_h \right.$$
$$\left. + \frac{\alpha_{\boldsymbol{u}}}{\delta_{\boldsymbol{u}\kappa}} \sum_{\boldsymbol{v}} \sum_{\boldsymbol{x}} g^{\boldsymbol{v}_{\boldsymbol{u}}} \eta_{\boldsymbol{u}\boldsymbol{x}} \theta_{\boldsymbol{u}}^{\boldsymbol{v}}(h^{(-1)}) \left[\kappa_{\boldsymbol{u}}(h^{(-1)} - t_{\boldsymbol{x}}) - \kappa_{\boldsymbol{u}}(h - t_{\boldsymbol{x}})\right] \right\}, \qquad (22)$$

where h represents the event time of any event $\boldsymbol{y}$ in the whole available history $\mathcal{D} = \cup_{\boldsymbol{u}} \mathcal{D}_{\boldsymbol{u}}^{(T_{\boldsymbol{u}})}$, $h^{(-1)}$ represents the last event time prior to h, and Δ_h is the difference between h and h^{-1}. Note that, we have $h^{(-1)} = 0$ for the first event time h.

Proof of Proposition 6.1. Using (4) – (8), we have the following:

$$\int_0^T \lambda_{\boldsymbol{u}}(z)dz = \int_0^T \mu_{\boldsymbol{u}}(z)dz + \int_0^T \sum_{\boldsymbol{v} \in I \times S} A_{\boldsymbol{u}}^{\boldsymbol{v}}(z) \sum_{\boldsymbol{x} \in \mathcal{D}_{\boldsymbol{v}}^{(z)}} \eta_{\boldsymbol{u}\boldsymbol{x}} \cdot \kappa_{\boldsymbol{u}}(z - t_{\boldsymbol{x}}) \qquad (23)$$

$$= \int_0^T \mu_{\boldsymbol{u}}(z)dz + \alpha_{\boldsymbol{u}} \sum_{\boldsymbol{v}} \sum_{\boldsymbol{x}} g_{\boldsymbol{u}}^{\boldsymbol{v}} \eta_{\boldsymbol{u}\boldsymbol{x}} \int_0^T \theta_{\boldsymbol{u}}^{\boldsymbol{v}}(z)\kappa_{\boldsymbol{u}}(z - t_{\boldsymbol{x}})dz \qquad (24)$$

$$= \sum_{h \in \{t_{\boldsymbol{y}} | \boldsymbol{y} \in \mathcal{D}\}} \left\{ \mu_{\boldsymbol{u}}(h^{-1})\Delta_h \right.$$
$$\left. + \frac{\alpha_{\boldsymbol{u}}}{\delta_{\boldsymbol{u}\kappa}} \sum_{\boldsymbol{v}} \sum_{\boldsymbol{x}} g_{\boldsymbol{u}}^{\boldsymbol{v}} \eta_{\boldsymbol{u}\boldsymbol{x}} \theta_{\boldsymbol{u}}^{\boldsymbol{v}}(h^{(-1)}) \left[\kappa_{\boldsymbol{u}}(h^{(-1)} - t_{\boldsymbol{x}}) - \kappa_{\boldsymbol{u}}(h - t_{\boldsymbol{x}})\right] \right\}, \qquad (25)$$

where h represents the event time of any event $\boldsymbol{y}$ in the whole available history $\mathcal{D} = \cup_{\boldsymbol{u}} \mathcal{D}_{\boldsymbol{u}}^{(T_{\boldsymbol{u}})}$, $h^{(-1)}$ represents the last event time prior to h, and Δ_h is the difference between h and h^{-1}. Note that, we have $h^{(-1)} = 0$ for the first event time h. ∎

Proposition 6.1 allows us to tractably integrate the intensity function $\lambda_{\boldsymbol{u}}(t)$ under mild assumptions on the data-generating processes, which is common in geospatial statistics, including spatio-temporal point process models [Meyer et al., 2012, Chiang et al., 2022]. Note that one could also consider numerical integration to estimate the integral in 10.

We note that STEMMED is considered as a 1-dimensional point process model, as we are only concerned with temporal event streams for community-cause-of-death pairs. As a result, we only integrate over the temporal space in the log-likelihood function. On the contrary, higher dimensional point process models that incorporate the whole geographic space and the marked space suffer from the so-called curse of dimensionality as the integral in their log-likelihood functions would be analytically intractable or computationally formidable with numerical integration Reinhart [2018]. More specifically, although in STEMMED, $g_{\boldsymbol{u}}^{\boldsymbol{v}}$ and $\eta_{\boldsymbol{u}\boldsymbol{x}}$ account for spatial effects and personalized triggering effects, respectively, these components only amplify or attenuate past events' influences to current "time" instead "mark-space-time," which also allows us to compute the integral more efficiently.

Continuous-time Forecasting Procedure. The continuous-time version of the multi-period ahead prediction algorithm is summarized in Algorithm 2. It is based on the simulation technique of Point Processes or the Ogata's modified thinning algorithm.

STEMMED-based online Forecasting Framework. We extend the STEMMED-based multi-period cooperative forecasting algorithm to an online setting (Algorithm 3).

Summary of data used in the case study

Event-level Data. We obtained individual-level data for deaths recorded from January 1, 2015, to July 31, 2021, from the Massachusetts Registry of Vital Records and Statistics. We used ICD-10-CM codes to identify the five underlying

---
Algorithm 2 Continuous Time Multi-Period Prediction (based on Ogata's Thinning Algorithm)

    Input: $\mathcal{D}, t, T, \lambda_{\boldsymbol{u}}(t)$
    Output: $\mathcal{D}$
1: $\lambda \leftarrow 0, \tilde{\lambda} \leftarrow 0, \delta \leftarrow 0, \text{accept} \leftarrow 0, m \leftarrow (0,0), \boldsymbol{p} \leftarrow \boldsymbol{0}, \boldsymbol{x} \leftarrow \boldsymbol{0}.$
2: **while** $t \leq T$ **do**
3:     $\lambda \leftarrow \sum_{\boldsymbol{u} \in I \times S} \lambda_{\boldsymbol{u}}(t^{+})$
4:     $\delta \leftarrow$ Sample from *Exponential*$(1/\lambda)$
5:     $t \leftarrow t + \delta$
6:     $\tilde{\lambda} \leftarrow \sum_{\boldsymbol{u} \in I \times S} \lambda_{\boldsymbol{u}}(t)$
7:     accept $\leftarrow$ Sample from *Bernoulli*$(\tilde{\lambda}/\lambda)$
8:     **if** accept $= 1$ **then**
9:         **for** $\boldsymbol{u} \in I \times S$ **do**
10:           $(\mathbf{p})_{\boldsymbol{u}} \leftarrow \lambda_{\boldsymbol{u}}(t)/\tilde{\lambda}$
11:         **end for**
12:         $\hat{\boldsymbol{u}} \leftarrow$ Sample from *Multinomial*$(\mathbf{p})$
13:         $\boldsymbol{m}_{\boldsymbol{u}}^{\text{new}} \leftarrow f(\boldsymbol{m}|\mathcal{D}_{i,s}^{(t)})$
14:         $\boldsymbol{x}_{\boldsymbol{u}}^{\text{new}} \leftarrow (t, \boldsymbol{m}_{\boldsymbol{u}}^{\text{new}})$
15:     **end if**
16:     $\mathcal{D} \leftarrow \mathcal{D} \bigcup \{\boldsymbol{x}_{\boldsymbol{u}}^{\text{new}}\}$
17: **end while**

Algorithm 3 STEMMED-based Online Cooperative Forecasting Framework
---
    Input: $t, \mathcal{D}^{(t)}, \{\lambda_{\boldsymbol{u}} \mid \boldsymbol{u} \in I \times S\}, T, M, n, l > 0$
    Output: $\mathcal{D}^{(T)}$
1: **while** $t \leq T$ **do**
2:     **for** $\boldsymbol{u} \in I \times S$ **do**
3:         Update $\lambda_{\boldsymbol{u}}$ by solving (10)
4:     **end for**
5:     **while** $t^{\text{new}} = t + n, t + 2n, \ldots,$ and $t^{\text{new}} \leq t + M$ **do**
6:         **for** $\boldsymbol{u} \in I \times S$ **do**
7:           Update $\mathcal{D}^{(t^{\text{new}})}$
8:         **end for**
9:         $\mathcal{D}^{(t^{\text{new}}+l)} \leftarrow$ Predictions made by Algorithm 1 with l being the forecasting horizon
10:     **end while**
11:     $t \leftarrow t + M$
12: **end while**
---

causes of death involving opioid-overdose: T40.1 (Heroin), T40.2 (prescription opioids), T40.3 (Methadone), T40.4 (Fentanyl and its derivatives), and T40.6 (other unspecified narcotics). In addition to the underlying causes of death, this dataset contains a subset of information appearing on decedents' death certificates, including location and time of death and other individual-level socioeconomic information such as age, gender, and race. Table 3 shows the summary of the data collected for the case study.

Additional Retrospective Analyses

In addition to the analyses in Section 5.2.3, we observed that past events from Middlesex, Worcester, and Suffolk had the largest impacts on the number of expected OOD events in Norfolk during the study period. While the effects from Middlesex peaked at December 2017 to around 25% of the expected OOD events, these effects generally explained around 15% of the expected amount OOD events. It also shows that these effects from Worcester had gradually increased from 5% to 15% in 6 years. For the public health department in Norfolk, these observations may suggest a need to perform thorough investigations into the connections between the events in these counties to design suitable cross-region intervention measures. On the other hand, triggering effects to Suffolk did not impact the county as much as the triggering effects to other counties (See Figure 4 for a clearer view).

Table 3: Summary of opioid-involved overdose deaths in the state of Massachusetts ranging from January 1, 2015 to July 31, 2021.

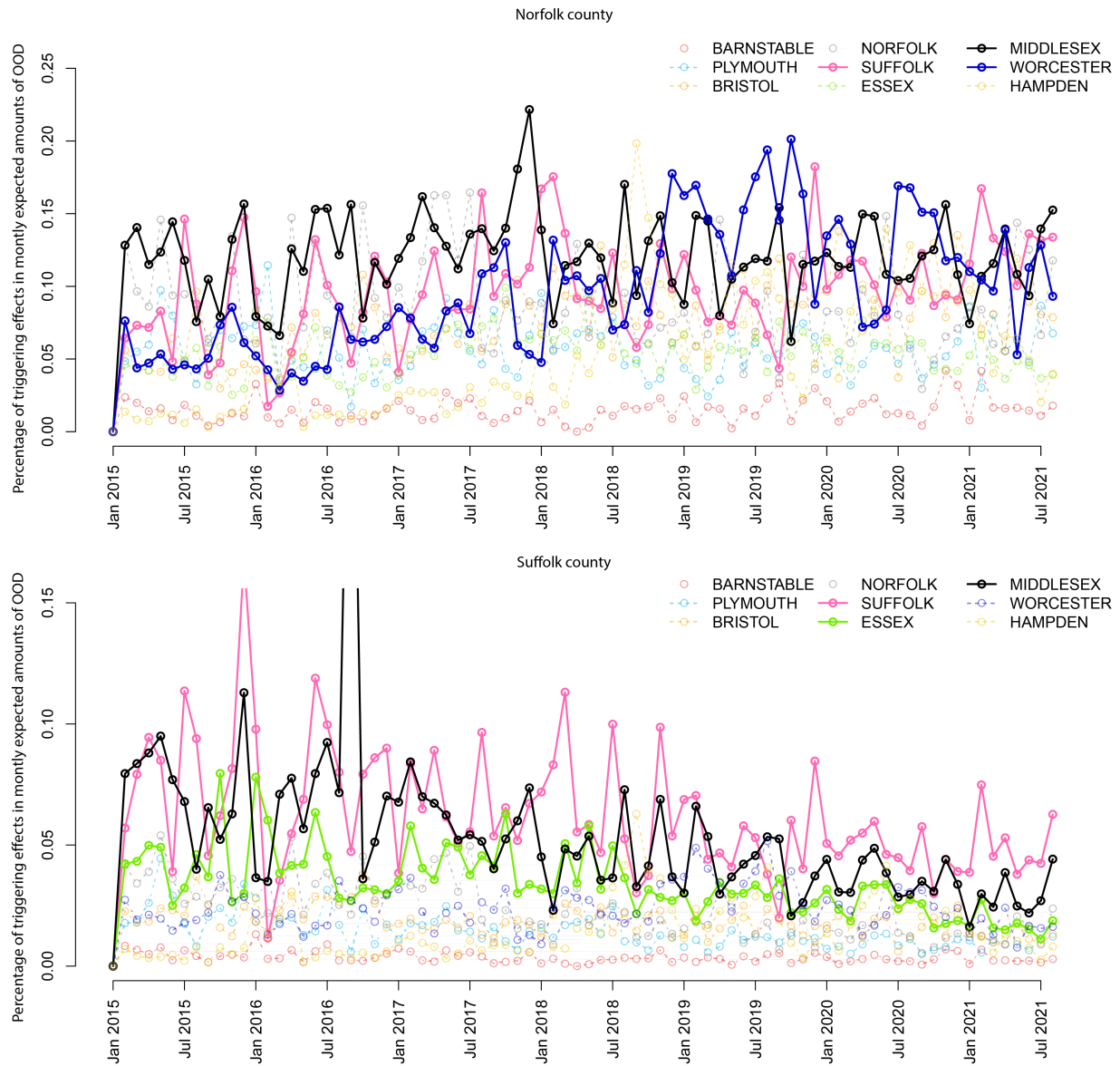|	Count	(Proportion)
Total Overdose Deaths	13233	
Underlying Causes of Death (ICD-10 Code)		
Heroin (T40.1)	3,049	
Prescription Opioids (T40.2)	1,695	
Methadone (T40.3)	608	
Fentanyl (T40.4)	11,319	
Unspecified Narcotics (T40.6)	1,508	
Poly-Substance Involvement		
1	9,261	69.9%
2	3,120	23.5%
3	731	5.5%
4	120	0.9%
5	1	0.007%
County		
Middlesex	2,174	16.4%
Suffolk	1,962	14.8%
Worcester	1,726	13%
Essex	1,713	12.9%
Bristol	1,521	11.5%
Hampden	1,132	8.5%
Plymouth	1,021	7.7%
Norfolk	950	7.1%
Barnstable	456	3.4%
Berkshire	267	2%
Hampshire	183	1.3%
Franklin	99	0.7%
Dukes	19	0.1%
Nantucket	10	0.07%
Age		
Age ≤ 18	53	4.0%
$18 < $ Age ≤ 30	2,972	22.4%
$30 < $ Age ≤ 40	3,909	30%
$40 < $ Age ≤ 50	2,965	22.4%
Age > 50	3,334	25.2%
Sex		
Male	9,747	73.6%
Female	3,486	26.3%
Race		
White, non-Hispanic	10,505	79.37%
Hispanic	1,640	12.39%
Black, non-Hispanic	778	5.88%
Asian, non-Hispanic	109	0.83%
Others, or Unknown	211	1.59%

Figure 4: The percentages of triggering effects in the expected total OOD events of Norfolk County and Suffolk County, from January 1, 2015, to August 1, 2021.